Resolution of the Gross-Pitaevskii equation with the imaginary-time method on a Lagrange mesh

D. Baye* and J.-M. Sparenberg†
Physique Quantique, C.P. 165/82 and Physique Nucléaire Théorique et Physique Mathématique, C.P. 229, Université Libre de Bruxelles, B 1050 Brussels, Belgium
(Received 9 August 2010; published 1 November 2010)

The Lagrange-mesh method is an approximate variational calculation which has the simplicity of a mesh calculation. Combined with the imaginary-time method, it is applied to the iterative resolution of the Gross-Pitaevskii equation. Two variants of a fourth-order factorization of the exponential of the Hamiltonian and two types of mesh (Lagrange-Hermite and Lagrange-sinc) are employed and compared. The accuracy is checked with the help of these comparisons and of the virial theorem. The Lagrange-Hermite mesh provides very accurate results with short computing times for values of the dimensionless parameter of the nonlinear term up to 10^4. For higher values up to 10^7, the Lagrange-sinc mesh is more efficient. Examples are given for anisotropic and nonseparable trapping potentials.

DOI: 10.1103/PhysRevE.82.056701 PACS number(s): 02.70.Hm, 03.75.Hh, 02.70.Jn, 31.15.−p

I. INTRODUCTION

The Gross-Pitaevskii equation describes the behavior of a Bose-Einstein condensate at zero temperature within the mean-field approximation [1]. This nonlinear Schrödinger equation involves an external trapping potential and a nonlinear term due to the interactions between atoms. The atom-atom interaction within the dilute condensate is modeled only by its scattering length. The common individual wave function of each boson of the condensate is a self-consistent solution of this equation.

Accurate numerical techniques for the resolution of the three-dimensional Gross-Pitaevskii equation have been proposed in a number of papers [2–10]. The goal of the present study is to derive an approach which is both fast and very accurate. This approach is based on several well established ingredients, i.e., the imaginary-time method, a fourth-order factorization algorithm of the imaginary-time propagator [8], and the Lagrange-mesh method [11–13].

The imaginary-time method is used in many subfields of quantum physics and in particular to solve the Gross-Pitaevskii equation [4,8]. This method has been made very efficient with the use of high-order factorizations of the exponential imaginary-time propagator. This factorization has been the subject of many theoretical [8,14–18] and numerical works [18,19]. A fourth-order factorization algorithm is well adapted to an accurate resolution of the Gross-Pitaevskii equation [8]. Higher-order algorithms are more accurate but their additional complication and computer-time cost do not make them optimal [19].

The Lagrange-mesh method is an approximate variational method which resembles a mesh calculation because of the use of a consistent Gauss quadrature [11–13]. The numerical calculation is similar to the one obtained within the discrete-variable representation (DVR) employed in Ref. [2]. The difference lies in the use of variational functions vanishing at all points but one of a mesh. In its simplest variant, the Lagrange-mesh method is equivalent to the DVR (and a little simpler) when the mesh points are zeros of orthogonal polynomials. The Lagrange-mesh method allows very accurate calculations in various problems of nuclear and atomic physics. In particular, it provides in a simple way very accurate energies and wave functions for three-body atoms and molecules and for simple atomic and molecular systems in strong magnetic fields [20–24]. All these applications involve linear operators. Here we extend this technique to a nonlinear equation.

The originality of the present approach lies in the combined use of known ingredients to obtain a simple technique of resolution of the three-dimensional nonlinear Gross-Pitaevskii equation. We employ two different Lagrange meshes based on Hermite polynomials and on sinc functions with two variants of fourth-order factorization algorithm. In Ref. [2], a DVR based on Hermite polynomials is also employed, but leads to less accurate results in spite of larger numbers of basis functions. In Ref. [4], Hermite polynomials are employed analytically with a second-order factorization algorithm. The efficiency of a fourth-order algorithm is established in Ref. [8] with a finite-difference technique. The factorization algorithm of the propagation operator takes a very simple form when adapted to Lagrange functions with the consistent Gauss approximation [18,19] and leads to a fast and accurate method.

In Sec. II, we recall the Gross-Pitaevskii equation in reduced units and summarize some of its properties. The Lagrange-mesh method is presented and details are given about the Lagrange-Hermite and Lagrange-sinc meshes. Variants of the imaginary-time method are then discussed in the context of the Lagrange-mesh method. In Sec. III, the conditions of the calculations and the accuracy of the results are discussed. The method is applied to isotropic and anisotropic harmonic-oscillator potentials and to a nonseparable potential. Concluding remarks are presented in Sec. IV.

II. THEORY

A. Gross-Pitaevskii equation

In the absence of interaction between the bosons, their wave function is an eigenfunction of the "external" Hamiltonian

*dbaye@ulb.ac.be
†jmspar@ulb.ac.be

$$H_{\rm ext} = -\frac{1}{2}\Delta + V_{\rm ext} \tag{1}$$

with $\hbar = m = 1$. In this expression, $V_{\rm ext}$ is the external trapping potential. In most descriptions of experiments, this potential is well approximated by an oscillator trap

$$V_{\rm ext}^{\rm HO} = \frac{1}{2}(\omega_x^2 x^2 + \omega_y^2 y^2 + \omega_z^2 z^2). \tag{2}$$

The angular frequencies ω_x, ω_y, ω_z are expressed as a function of some additional unit $\omega = 1$. Hence the length and energy units are the harmonic-oscillator units, $(\hbar/m\omega)^{1/2}$ and $\hbar\omega$, respectively.

Under the assumption of a dilute system, the behavior of a condensate containing n bosons is described with the wave function ψ which is the normed ground-state solution of the Gross-Pitaevskii equation [1],

$$(H_{\rm ext} + \lambda|\psi(x,y,z)|^2)\psi(x,y,z) = \mu\psi(x,y,z). \tag{3}$$

The dimensionless parameter in the nonlinear term is defined as

$$\lambda = 4\pi n a\sqrt{\frac{m\omega}{\hbar}} \tag{4}$$

where a is the scattering length. Parameter λ can be positive or negative according to whether the interaction is repulsive or attractive. For example, in a spherical condensate of sodium atoms [2], this parameter reads

$$\lambda \approx 6.6 \times 10^{-5} n\sqrt{\omega}, \tag{5}$$

where ω is expressed in s^{-1}.

The eigenvalue μ in Eq. (3) is the chemical potential. It is also given by the expression

$$\mu = \langle H_{\rm ext}\rangle + \lambda\langle|\psi|^2\rangle, \tag{6}$$

which is useful when Eq. (3) is not solved directly. The energy per boson is given by the expression

$$E = \langle H_{\rm ext}\rangle + \frac{1}{2}\lambda\langle|\psi|^2\rangle. \tag{7}$$

The kinetic, external and interaction energies satisfy a virial theorem which is conveniently written under the form

$$E + \mu - 2\langle V_{\rm ext}\rangle - \langle \boldsymbol{r}\cdot\boldsymbol{\nabla}V_{\rm ext}\rangle = 0. \tag{8}$$

It will serve as a test of the accuracy of the numerical calculations. The last term is easily computed within the Lagrange-mesh method. For the harmonic confinement [Eq. (2)], this theorem becomes [1]

$$E + \mu - 4\langle V_{\rm ext}^{\rm HO}\rangle = 0. \tag{9}$$

When the kinetic energy term can be neglected in Eq. (3), one obtains the Thomas-Fermi approximation which gives for a triaxial harmonic-oscillator trap [5]

$$\mu_{\rm TF} = \frac{1}{2}\left(\frac{15\lambda\omega_x\omega_y\omega_z}{4\pi}\right)^{2/5} \tag{10}$$

and

$$E_{\rm TF} = \frac{5}{7}\mu_{\rm TF}. \tag{11}$$

The validity of this approximation will also be tested in the following.

B. Lagrange-mesh method

1. Generalities

The Lagrange-mesh method is an approximate variational method displaying the simplicity of a calculation on a grid. Its ingredients are a set of N mesh points u_j, a Gauss quadrature approximation consistent with this mesh

$$\int_{-\infty}^{\infty} g(u)du \approx \sum_{j=1}^{N} \lambda_j g(u_j) \tag{12}$$

with weights λ_j, and N infinitely differentiable functions $f_i(u)$ associated with each mesh point satisfying the Lagrange conditions

$$f_i(u_j) = \lambda_i^{-1/2}\delta_{ij} \tag{13}$$

[see Eqs. (17) and (22) below]. The crucial property of the Lagrange functions is that Eqs. (12) and (13) imply

$$\int_{-\infty}^{\infty} f_i(u)f_{i'}(u)du \approx \delta_{ii'} \tag{14}$$

and

$$\int_{-\infty}^{\infty} f_i(u)V(u)f_{i'}(u)du \approx V(u_i)\delta_{ii'}. \tag{15}$$

The Lagrange basis can thus be treated as orthonormal (the bases used below are in fact strictly orthonormal) and the potential matrix is approximated by a diagonal expression. In spite of the Gauss approximation, the method is very accurate with small numbers of mesh points when $V(u)$ and its derivatives have no singularity [12,13].

The Lagrange functions are used to determine the kinetic-energy matrix elements associated with the mesh. The expressions of these matrix elements are simple [11,13] [see Eqs. (19) and (23) below]. The explicit expression of the Lagrange functions is mainly needed to compute the variational wave functions. Otherwise, because of the Lagrange property [Eq. (13)], they do not appear in calculations of eigenvalues and of mean values of observables which can be calculated with the Gauss quadrature [Eq. (12)].

The number of simple Lagrange functions and associated meshes satisfying the Lagrange condition (13) and for which the orthogonality [Eq. (14)] is exact is rather limited [13]. The choice of Lagrange basis is first determined by the interval of definition. Since we work here on $(-\infty,\infty)$, only two simple meshes are available: the Lagrange-Hermite mesh [11,13] constructed from the Hermite orthogonal polynomials and the Lagrange-sinc mesh [13] based on sinc interpolation functions. Another possibility would be the Lagrange mesh based on shifted Gaussian functions [25] but it is constructed from non standard orthogonal polynomials and thus more complicated to use.

2. Lagrange-Hermite mesh

As mentioned above, several Lagrange meshes are available on the interval $(-\infty,\infty)$ [13]. The choice can be fixed with some physical property. For a weak nonlinearity, the oscillator confinement suggests to use the Lagrange-Hermite mesh [11,13] defined by

$$H_N(u_j) = 0 \tag{16}$$

with the N index values $j=-\frac{1}{2}(N-1),\ldots,\frac{1}{2}(N-1)$. The corresponding quadrature is thus Gauss-Hermite which defines the weights λ_j [26]. Like Lagrange functions, these weights are only necessary to evaluate values of wave functions but they disappear from matrix elements. The corresponding Lagrange functions read [11]

$$f_i(u) = (-1)^{N+i}(\sqrt{\pi}2^{N+1}N!)^{-1/2}\frac{H_N(u)}{u-u_i}e^{-u^2/2}. \tag{17}$$

They are exactly orthogonal since the Gauss quadrature is exact for Eq. (14). The matrix elements of the operator $-d^2/du^2$ are given at the Gauss-Hermite approximation by

$$T_{ii'} = -\int_0^\infty f_i(u)f_{i'}''(u)du \approx -\lambda_i^{1/2}f_{i'}''(u_i), \tag{18}$$

i.e.,

$$T_{i\neq i'} = (-1)^{i-i'}\frac{2}{(u_i-u_{i'})^2},$$

$$T_{ii} = \frac{1}{3}(2N+1-u_i^2). \tag{19}$$

These expressions only depend on the mesh points u_i.

3. Lagrange-sinc mesh

For a strong nonlinearity, the condensate wave functions may be rather different from harmonic-oscillator functions. Hence we also choose the Lagrange-sinc mesh [13] involving equidistant mesh points

$$u_j = j, \quad j = -\frac{1}{2}(N-1),\ldots,\frac{1}{2}(N-1), \tag{20}$$

with the same labels as for the Hermite mesh. Switching the meshes is thus very easy. The corresponding weights are

$$\lambda_j = 1/N. \tag{21}$$

The Lagrange-sinc functions are defined by [13]

$$f_i(u) = \mathrm{sinc}(u-u_i) = \frac{\sin\,\pi(u-u_i)}{\pi(u-u_i)}. \tag{22}$$

Here also, they are exactly orthogonal and the Gauss approximation (14) is exact. The matrix elements of $-d^2/du^2$ are also given by Eq. (18) as

$$T_{i\neq i'} = (-1)^{i-i'}\frac{2}{(u_i-u_{i'})^2},$$

$$T_{ii} = \frac{\pi^2}{3}. \tag{23}$$

4. Parity projection and scaling

We assume that the potential is even with respect to $u\to -u$. Choosing N even for simplicity, we perform a parity projection of the Lagrange functions

$$f_i^p(u) = 2^{-1/2}[f_i(u) + pf_{-i}(u)] \tag{24}$$

with $p=\pm 1$ and $i=\frac{1}{2},\ldots,\frac{1}{2}(N-1)$. For parity p, the matrix elements of $-d^2/du^2$ are simply given for $i,i'>0$ by

$$T_{ii'}^p = T_{ii'} + pT_{i-i'}. \tag{25}$$

The potential matrix elements are unchanged,

$$\int_{-\infty}^{\infty} f_i^p(u)V(u)f_{i'}^{p'}(u)du \approx V(u_i)\delta_{ii'}\delta_{pp'}. \tag{26}$$

It is useful to consider the scaled mesh hu_j involving the scaling parameter h which allows fitting the mesh to the physical extension of the wave function. The normed Lagrange functions become $h^{-1/2}f_i^p(x/h)$. They satisfy the Lagrange property

$$h^{-1/2}f_i^p(u_j) = (2h\lambda_i)^{-1/2}\delta_{ij}. \tag{27}$$

For parity p, the Hamiltonian matrix reads

$$H_{ii'}^p = \frac{1}{2}h^{-2}T_{ii'}^p + V(hu_i)\delta_{ii'}. \tag{28}$$

5. Three-dimensional mesh

Let us now turn to the three-dimensional problem [Eq. (3)]. The potential is assumed to be even with respect to $\boldsymbol{r}\to-\boldsymbol{r}$. Let us consider three sets of N_x, N_y, N_z Lagrange functions $f_i^{p_x}(u)$, $g_j^{p_y}(v)$, $h_k^{p_z}(w)$ with parities p_x, p_y, p_z, respectively. The corresponding weights are λ_i, μ_j, ν_k. Introducing three scaling parameters h_x, h_y, h_z, one obtains the three-dimensional mesh (h_xu_i,h_yv_j,h_zw_k). Normed three-dimensional Lagrange functions can be defined as the products

$$F_{ijk}^{p_xp_yp_z}(x,y,z) = (h_xh_yh_z)^{-1/2}f_i^{p_x}(x/h_x)g_j^{p_y}(y/h_y)h_k^{p_z}(z/h_z). \tag{29}$$

They verify the Lagrange property

$$F_{ijk}^{p_xp_yp_z}(h_xu_{i'},h_yv_{j'},h_zw_{k'}) = (8h_xh_yh_z\lambda_i\mu_j\nu_k)^{-1/2}\delta_{ii'}\delta_{jj'}\delta_{kk'}. \tag{30}$$

The wave function of the condensate with parities p_x, p_y, p_z is then approximated as

$$\psi^{p_x p_y p_z}(x,y,z) = \sum_{i=1/2}^{1/2(N_x-1)} \sum_{j=1/2}^{1/2(N_y-1)} \sum_{k=1/2}^{1/2(N_z-1)} c_{ijk} F_{ijk}^{p_x p_y p_z}(x,y,z). \tag{31}$$

With Eq. (30), the values of the wave functions at mesh points are

$$\psi^{p_x p_y p_z}(h_x u_i, h_y v_j, h_z w_k) = (8 h_x h_y h_z \lambda_i \mu_j \nu_k)^{-1/2} c_{ijk} \tag{32}$$

and provide a simple physical interpretation of the coefficients c_{ijk}.

The matrix elements of Hamiltonian (1) are given by

$$\begin{aligned} H_{ijk,i'j'k'}^{p_x p_y p_z} = & \frac{1}{2} h_x^{-2} T_{ii'}^{p_x} \delta_{jj'} \delta_{kk'} + \frac{1}{2} h_y^{-2} \delta_{ii'} T_{jj'}^{p_y} \delta_{kk'} \\ & + \frac{1}{2} h_z^{-2} \delta_{ii'} \delta_{jj'} T_{kk'}^{p_z} \\ & + V_{\text{ext}}(h_x u_i, h_y v_j, h_z w_k) \delta_{ii'} \delta_{jj'} \delta_{kk'}, \end{aligned} \tag{33}$$

where $T_{ii'}^{p_x}$, $T_{jj'}^{p_y}$, and $T_{kk'}^{p_z}$ are given by expression (25). The matrix representing the external potential is diagonal. The nonlinear term is also diagonal,

$$\langle F_{ijk}^{p_x p_y p_z} | \lambda (\psi^{p_x p_y p_z})^2 | F_{i'j'k'}^{p_x p_y p_z} \rangle = \frac{\lambda c_{ijk}^2}{8 h_x h_y h_z \lambda_i \mu_j \nu_k} \delta_{ii'} \delta_{jj'} \delta_{kk'}. \tag{34}$$

The simple structures of Eqs. (33) and (34) are the main causes of the simplicity of the numerical algorithm described below.

C. Imaginary-time method

In order to solve the nonlinear Eq. (3), it is convenient to use the imaginary-time method which allows searching the lowest eigenvalue and looking for self-consistency in the same iterations. This algorithm is based on a separation of the linear or nonlinear operator into two parts,

$$H = H_{\text{ext}} + \lambda \psi^2 = H_0 + V, \tag{35}$$

where we assume that the wave function is real. We consider two cases in the following. In case a, H_0 is the operator H_{ext} defined in Eq. (1) and V is then the nonlinear term in Eq. (3),

$$H_0 = H_{\text{ext}}, \quad V = \lambda \psi^2. \tag{36}$$

In case b, H_0 is the kinetic energy operator and V is the sum of the external potential and of the nonlinear term,

$$H_0 = -\frac{1}{2}\Delta, \quad V = V_{\text{ext}} + \lambda \psi^2. \tag{37}$$

Intermediate choices are also possible.

The imaginary time $\Delta\tau$ appears as a parameter in an exponential of the Hamiltonian, $e^{-\Delta\tau H}$ which progressively extracts the ground-state component from an initial function $\psi(0)$ when the procedure is repeated. After normalization, the function

$$\psi(\Delta\tau) = e^{-\Delta\tau H} \psi(0), \tag{38}$$

where H depends on τ, is closer to the ground-state wave function than $\psi(0)$. If one uses small time steps $\Delta\tau$, one can modify the nonlinear term consistently and so approach self-consistency.

The exponential of H is not simple to compute. It is thus useful to resort to factorization algorithms, i.e., to approximations involving products of exponentials of simpler operators. At first order, i.e., with an error of order $\Delta\tau$, one obtains the algorithm

$$\psi(\Delta\tau) = e^{-\Delta\tau H_0} e^{-\Delta\tau V(0)} \psi(0). \tag{39}$$

The exponential of H_0 is calculated only once. The potential represented by V depends on the initial wave function. For example, in case a, it reads

$$V(0) = \lambda \psi(0)^2. \tag{40}$$

A second-order algorithm denoted as 2A in Ref. [8] reads

$$\psi(\Delta\tau) = e^{-1/2\Delta\tau V(\Delta\tau)} e^{-\Delta\tau H_0} e^{-1/2\Delta\tau V(0)} \psi(0). \tag{41}$$

In principle, the potential in the left factor should be $V(\Delta\tau)$. When it is replaced by $V(0)$, one obtains the algorithm 2A0 of Ref. [8] with an error of order $\Delta\tau^2$. Its implementation is not more difficult than at first order. Notice that we have tested the suggestion of Ref. [8] to use a Lambert function in version 2A of the algorithm to better approximate $V(\Delta\tau)$. We have found some enlargement of the range of $\Delta\tau$ values for which the algorithm converges but only for not too strong nonlinear terms. The simpler algorithm 2A0 seems thus preferable in view of the fact that computation times are very short.

As suggested in Ref. [8], the fourth-order algorithm

$$\begin{aligned} \psi(\Delta\tau) = & e^{-(1/6)\Delta\tau V(\Delta\tau)} e^{-(1/2)\Delta\tau H_0} e^{-(2/3)\Delta\tau \tilde{V}(\Delta\tau/2)} \\ & \times e^{-(1/2)\Delta\tau H_0} e^{-(1/6)\Delta\tau V(0)} \psi(0) \end{aligned} \tag{42}$$

might be optimal by providing an error of order $\Delta\tau^4$ with reasonable computing times. This algorithm involves the modified potential

$$\tilde{V} = V + \frac{\Delta\tau^2}{48}[V,[H_0,V]] = V + \frac{\Delta\tau^2}{48}(\nabla V)^2. \tag{43}$$

In case b, ∇V reads

$$\nabla V = \nabla V_{\text{ext}} + 2\lambda \psi \nabla \psi. \tag{44}$$

The first term is calculated analytically and the second one requires the calculation of $\nabla\psi$. Type a only involves the second term. We show in the Appendix that $\nabla\psi$ can be obtained easily and accurately on a Lagrange mesh. In practice, we replace the potential evaluations at $\Delta\tau$ and $\Delta\tau/2$ by evaluations at zero as in Eq. (40). This leads to algorithm 4A00 of Ref. [8].

The algorithm involves exponentials of two types of matrices. On a Lagrange mesh, matrix V is diagonal. This is the case for any combination of the external potential [see Eqs. (26) or (33)] and of the non local term [see Eq. (34)]. The exponential is thus easily obtained and its multiplication with the vector representing the wave function is fast. On the

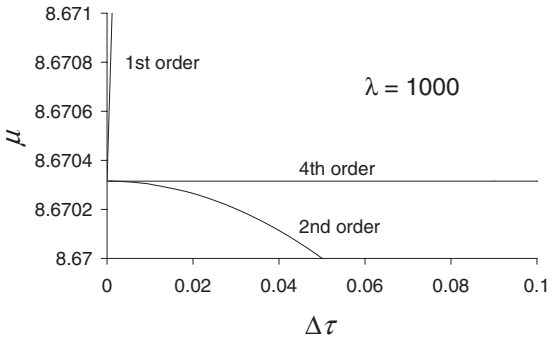

FIG. 1. Chemical potential as a function of $\Delta\tau$ for $\lambda=1000$ with the first-order, second-order 2A0, and fourth-order 4A00 algorithms.

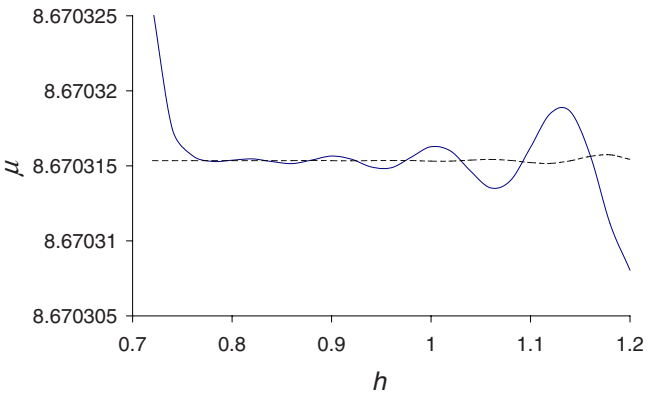

FIG. 2. (Color online) Dependence on the scaling parameter h for the Hermite mesh at $\lambda=1000$ with $N=30$ (full line) and $N=40$ (dashed line) mesh points ($\Delta\tau=0.05$).

other hand, matrix H_0 is nondiagonal. Since its expression does not depend on λ, its exponential can be obtained with a single diagonalization performed at the beginning of the algorithm. However, its multiplication with a vector would take $(N/2)^6$ multiplications which may be quite long (we assume $N_x=N_y=N_z=N$ to simplify the presentation). Fortunately the structure of this matrix [Eq. (33)] allows a significant simplification. The exponential operator can be written as

$$e^{-\Delta\tau H_0}=e^{-\Delta\tau H_{0x}}e^{-\Delta\tau H_{0y}}e^{-\Delta\tau H_{0z}}. \tag{45}$$

Each operator H_{0x}, H_{0y}, H_{0z} acts on a single coordinate. Its matrix representation is an $N/2\times N/2$ matrix which is diagonalized only once. The multiplication by the three matrices corresponding to the operators in the right-hand side of Eq. (45) requires only $3(N/2)^4$ multiplications per iteration. The calculation of the gradient takes about the same time as the application of one exponential in Eq. (45) and leads to a total of about $4(N/2)^4$ multiplications per iteration. This algorithm is thus very fast. It remains fast when the trapping potential is non separable if H_0 is chosen as the kinetic energy (case b).

To illustrate the difference between the algorithms at various orders, we display in Fig. 1 the dependence of their results on the choice of $\Delta\tau$. The calculations are performed for $\lambda=1000$ in case a. The first, second, and fourth-order behaviors are confirmed. Similar behaviors can be observed in Figs. 1–3 of Ref. [8].

III. RESULTS

A. Conditions of the calculation

First, we describe the procedure. Let us start with the spherical case. The three directions are described with the same number N of mesh points and the same scaling parameter h. Switching to an anisotropic confinement is rather easy as discussed below. We use the fourth-order algorithm throughout.

For each value of λ, we have various options. For H_0 we can use the oscillator Hamiltonian (case a) or the kinetic energy (case b). And we can use either the Hermite or the sinc mesh. The starting point of the iteration is the harmonic-oscillator wave function for $\lambda\leq 10^3$ and the Thomas-Fermi approximation for $\lambda>10^3$.

In each case, there are three parameters to choose: the common number N of mesh points and scaling parameter h in each direction, and the imaginary-time step $\Delta\tau$. Except for h, which must be rather roughly optimized, the choice of the other parameters depends on the searched for accuracy. Since we are testing a method, we shall try to obtain the best accuracy for reasonable computing times. Since this accuracy will often exceed physical needs, the practical computing will in general be even shorter.

The choice of h is illustrated for the Hermite mesh in Fig. 2. The calculation is performed for $\lambda=1000$ with $\Delta\tau=0.05$ for $N=30$ (full line) and $N=40$ (dashed line). One observes that for given N and $\Delta\tau$, the results are very stable over a plateau of h values: about six digits between 0.78 and 1 for $N=30$ and about eight digits between 0.72 and 0.98 for $N=40$. However the fact that, because of the Gauss quadrature approximation, the method is not really variational clearly appears in the oscillations and in the drop for high h. The virial theorem is a good indicator of the accuracy (see below). For $N=30$, it suggests that $h=0.8$ is optimal, a fact confirmed by the comparison with $N=40$ in Fig. 2. A similar figure is obtained for the energy per boson E with, however, a smaller extension of the oscillations (by more than an order of magnitude).

The convergence with respect to the number N of mesh points is illustrated for the Hermite mesh in Fig. 3. The calculations are performed for $\lambda=1000$ with $\Delta\tau=0.01$ and the optimal parameter $h=0.8$. The error $\epsilon_\mu=|\mu-\mu_{\text{exact}}|$ on the chemical potential, where the exact value μ_{exact} is approximated by a calculation with $N=50$, i.e., 8.670 315 355 7, is depicted with squares as a function of N. The convergence is approximately exponential from $N=10$ to about 26–30. Beyond $N=30$, the accuracy still improves but more slowly and the sign of the error starts varying. The absolute value of the virial residue, i.e., the left-hand member of Eq. (9), is represented by triangles in the same figure. Its decrease is also slower beyond about $N=30$ where the sign of this residue also starts changing. Strikingly, its behavior is qualitatively similar to the behavior of the error ϵ_μ so that this residue can

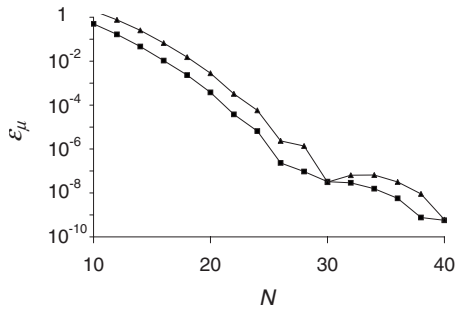

FIG. 3. Error $\epsilon_\mu=|\mu-\mu_{\text{exact}}|$ on the chemical potential (squares) and absolute value of the virial residue $|E+\mu-4\langle V_{\text{ext}}^{\text{HO}}\rangle|$ (triangles) for the Hermite mesh at $\lambda=1000$ as a function of the number N of mesh points with $h=0.8$ and $\Delta\tau=0.01$.

be considered as a good indicator of an improvement of accuracy. The additional computational cost of N values beyond about 30 does not lead to a significant enough improvement of the accuracy. In this sense, values close to $N=30$ can be considered as optimal.

Optimal choices of N and h are summarized as a function of λ for both meshes in Table I. Smaller values of N provide less accuracy but may of course be sufficient for physical applications while higher value of N do not lead to a much better accuracy. Since h weakly depends on λ, its choice can easily be obtained by interpolation between the values displayed in the table. Small variations around these values still lead to results of excellent accuracy except for the highest λ values considered.

The accuracy can also be tested as a function of $\Delta\tau$. An example is given in Table II where the chemical potential μ calculated with Eq. (6) and the energy per particle calculated with Eq. (7) are displayed for $\lambda=1000$ in case a with the Hermite mesh for $N=30$ and 40. The longest calculation (last line) took a few seconds on a 3.6 GHz personal computer. For this reason, we did not try to optimize the parameters further. The fact that the algorithm does not converge for larger $\Delta\tau$ values such as 0.2 is not a serious drawback.

One observes that the energy per particle converges faster than the chemical potential and is more accurate. We assume that this property is related to the variational origin of Eq. (7) for E. The energy per boson is already converged with

TABLE I. Values of N and h leading to highly accurate results (see Table III) as a function of λ.

	Lagrange-Hermite		Lagrange-sinc	
λ	N	h	N	h
1	20	0.9	20	0.5
10	20	0.8	30	0.4
10^2	26	0.8	30	0.4
10^3	30	0.8	40	0.35
10^4	50	1.0	50	0.45
10^5	70	1.15	60	0.45
10^6			70	0.5
10^7			80	0.7

TABLE II. Variation of accuracy for various choices of parameters for the fourth-order algorithm at $\lambda=1000$ with $h=0.8$ in case a with the Hermite mesh. The third column gives the number N_{iter} of iterations.

N	$\Delta\tau$	N_{iter}	E	μ	Virial
30	0.1	71	6.308834870	8.670315218	0.000000221
40	0.1	71	6.308834862	8.670315182	0.000000244
30	0.05	153	6.308834870	8.670315379	−0.000000012
40	0.05	154	6.308834862	8.670315346	0.000000018
30	0.02	372	6.308834870	8.670315388	−0.000000030
40	0.02	372	6.308834862	8.670315356	0.000000001
30	0.01	732	6.308834870	8.670315389	−0.000000031
40	0.01	730	6.308834862	8.670315356	0.000000001

$\Delta\tau=0.1$. With $N=30$, the error is of the order of 10^{-8} for E and four times larger for μ (we have checked that, with $N=40$, all displayed digits are converged). Another indication about the accuracy is given by the virial theorem [Eq. (9)] presented in the last column. The smallness of the virial residue is used as a guide for finding optimal conditions for the calculation. When this residue cannot be made small, it gives a rough estimate of the accuracy on the chemical potential.

B. Comparison of the different calculations

We compare in Table III calculations with reasonable numbers of mesh points as given in Table I for the four considered cases as a function of positive values of parameter λ. We could not obtain a convergence with the Hermite-mesh calculations for $\lambda>10^5$ with $N\leq 80$. The Thomas-Fermi approximation (TF) is also displayed for high λ.

For each λ value, four calculations are compared, i.e., factorizations a and b with either the Hermite or sinc mesh. The value of $\Delta\tau$ and the number of iterations N_{iter} are given. No attempt has been made to optimize them. The values of the virial expression (9) are also given. As expected convergence becomes more difficult when λ is very large because the nonlinear term becomes strongly dominant. Smaller $\Delta\tau$ values must be used. At $\lambda=10^7$, the error is still slightly smaller than the difference with the Thomas-Fermi approximation. The longest calculation (last lines) took less than two minutes. Other computation times can be estimated from the scaling law N^4N_{iter}.

A first general remark is that there is little difference between the two types of factorization. At small λ, type a is faster but computation times are negligible. In the whole range, the difference between the a and b results is smaller than the accuracy on these results. In other words, the a and b calculations provide the same accuracy but this accuracy cannot be derived from a comparison between them.

The difference between both types of Lagrange mesh is more significant. At small λ, the Hermite mesh is more accurate, especially in case a, as expected from the fact that this mesh is related to the harmonic oscillator [11] (for $\lambda=0$, it gives exact results with $N=2$ and $h=1$!). Around 10^3,

TABLE III. Chemical potential μ and energy E with optimal Hermite and sinc meshes (see Table I for N and h) for $\omega_x=\omega_y=\omega_z=1$. Cases a and b correspond to separations of H in Eqs. (36) and (37), respectively.

λ	Case	Mesh	$\Delta\tau$	N_{iter}	E	μ	Virial
1	a	Her.	0.05	106	1.530891280	1.560971500	−0.000000001
	b	Her.	0.05	287	1.530891280	1.560971500	0.000000020
	a	Sinc	0.05	265	1.530891280	1.560971499	−0.000000023
	b	Sinc	0.05	289	1.530891280	1.560971499	−0.000000002
10	a	Her.	0.05	213	1.757545057	1.973794544	0.000000006
	b	Her.	0.05	261	1.757545057	1.973794546	0.000000024
	a	Sinc	0.05	268	1.757545057	1.973794545	0.000000008
	b	Sinc	0.05	269	1.757545057	1.973794546	0.000000026
10^2	a	Her.	0.05	183	2.867920410	3.713215597	0.000000016
	b	Her.	0.05	220	2.867920410	3.713215601	0.000000037
	a	Sinc	0.05	218	2.867920410	3.713215590	−0.000000013
	b	Sinc	0.05	210	2.867920410	3.713215593	0.000000008
10^3	a	Her.	0.05	153	6.308834870	8.670315379	−0.000000012
	b	Her.	0.05	176	6.308834870	8.670315391	0.000000049
	a	Sinc	0.05	176	6.308834862	8.670315346	0.000000031
	b	Sinc	0.05	165	6.308834862	8.670315358	0.000000090
10^4	a	Her.	0.02	299	15.37747175	21.44602932	−0.00000105
	b	Her.	0.02	293	15.37747175	21.44602932	−0.00000105
	a	Sinc	0.02	299	15.37747165	21.44602901	−0.00000036
	b	Sinc	0.02	309	15.37747165	21.44602901	−0.00000037
	TF				15.2614	21.3660	
10^5	a	Her.	0.01	477	38.3909216	53.7068351	0.0000044
	b	Her.	0.01	410	38.3909216	53.7068351	0.0000044
	a	Sinc	0.01	457	38.3909220	53.7068354	−0.0000012
	b	Sinc	0.01	431	38.3909220	53.7068354	−0.0000012
	TF				38.339	53.6689	
10^6	a	Sinc	0.005	570	96.3193038	134.82776	0.00012
	b	Sinc	0.005	577	96.3193038	134.82776	0.00012
	TF				96.2930	134.8101	
10^7	a	Sinc	0.002	1130	241.8890989	338.6354	−0.0018
	b	Sinc	0.002	1134	241.8890989	338.6354	−0.0018
	TF				241.8770	338.6278	

the accuracies are comparable. Beyond 10^4, the sinc mesh becomes progressively more accurate. The Hermite mesh does not converge any more beyond 10^5.

The radial behavior of the corresponding spherical wave functions is displayed in Fig. 4. They are calculated with Eqs. (31), (29), and (17) or (22) for $x=y=0$. There is no visible difference between the four variants of calculation. At this scale, there is also essentially no difference with the Thomas-Fermi approximation beyond $\lambda=10^3$. For $\lambda=1$ and 10, the wave functions still resemble the harmonic-oscillator ground-state one. When λ increases, they become progressively flatter and more extended.

C. Attractive case

The condensate is still metastable in the attractive case when $|\lambda|$ is not too large [1,27]. Beyond the limit $\lambda\approx-7.226$, the condensate collapses within the present Gross-Pitaevskii approximation [27]. Results with case a for different values close to this limit are presented in Table IV. We have rather arbitrarily stopped calculations after 25 000 iterations.

When approaching the critical value, the convergence becomes very slow and requires many iterations. We were not

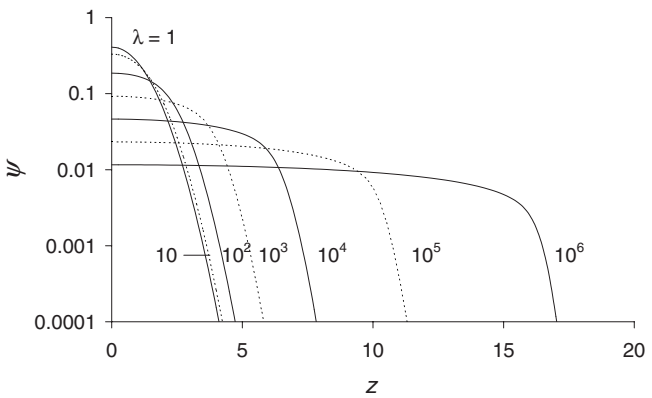

FIG. 4. Wave functions $\Psi(0,0,z)$ for $\omega=1$ and $\lambda=1$ to 10^6.

TABLE IV. Chemical potential μ and energy E in the attractive case with optimal Hermite and sinc meshes for $\omega_x=\omega_y=\omega_z=1$.

λ	Mesh	N	h	$\Delta\tau$	N_{iter}	E	μ	Virial
−7	Her.	40	0.55	0.01	4166	1.188408484	0.620438938	0.000000002
	Sinc	40	0.22	0.01	3997	1.188408502	0.620439934	−0.000000282
−7.1	Her.	40	0.55	0.01	5000	1.180003036	0.559434087	−0.000000021
	Sinc	40	0.22	0.01	5075	1.180003081	0.559437733	−0.000000900
−7.2	Her.	40	0.51	0.01	9950	1.170760551	0.45516550	−0.000000011
	Sinc	40	0.22	0.01	10004	1.170760620	0.4551696	0.000000774
−7.22	Her.	40	0.50	0.01	19745	1.168719451	0.40629052	0.000000018
	Sinc	40	0.20	0.01	19898	1.168719546	0.4063140	−0.000000102
−7.225	Her.	40	0.46	0.01	25000	1.16818287	0.3730864	0.00000008
	Sinc	40	0.20	0.01	25000	1.16818299	0.3731851	0.00000074
−7.2252	Her.	40	0.43	0.01	25000	1.16816093	0.368002	−0.0000003
	Sinc	40	0.19	0.01	25000	1.16816099	0.368127	−0.0000002
−7.2253	Her.	40	0.40	0.01	25000	1.1681508	0.36118	−0.000007
	Sinc	40	0.18	0.01	25000	1.1681505	0.36202	−0.000010
−7.2254	Her.	50	0.43	0.01	25000	1.1681372	0.3446	−0.0004
	Sinc	40	0.19	0.01	25000	1.1681375	0.3451	−0.0004

able to find significant results beyond −7.2254. Even this value is probably not a very accurate limit. We have used the virial expression to select the supposed optimal values of h. The comparison of the two meshes however shows that the accuracy on the chemical potential is less good than expected from the values of the virial expression. Anyway, one sees that the chemical potential drops rapidly.

The accuracy on the average energy per boson is again much better than for the chemical potential. This energy tends to a finite limit of about 1.1681.

D. Anisotropic-oscillator potential

As a trap, we now consider the anisotropic oscillator potential studied in Ref. [5], i.e., $\omega_x^2=0.3$, $\omega_y^2=0.6$, and $\omega_z^2=0.5$ after conversion into the present notation. Results with case a for various nonlinear parameters are presented in Table V. The conditions of the calculation are roughly interpolated from Table I (we keep $N_x=N_y=N_z$). Notice that since $\omega\neq 1$, the interpolation must be based on the effective value $\lambda/\sqrt{\omega}$ with $\omega^2\approx 0.5$. The values of the scaling parameters h_i are taken as $h/\sqrt{\omega_i}$ for $i=x$, y, z with h given by Table I for the effective value. In the units of Ref. [5], the dimensionless parameter is represented by 2λ and the chemical potential by 2μ. These values are converted into the present notation in Table V.

The convergence and accuracy are very similar to the spherical case. The computation times remain as short as in the isotropic case. The agreement with Ref. [5] is excellent up to $\lambda=5000$ (an obvious misprint has been corrected for $\lambda=50$). On the contrary, the results at 15 000 and 25 000 disagree at the 0.001 level. Since our results are stable with respect to variations of N, h, and $\Delta\tau$ and since the virial test

TABLE V. Chemical potential μ, energy E, and virial residue with the Hermite mesh for $\omega_x^2=0.3$, $\omega_y^2=0.6$, and $\omega_z^2=0.5$. The last column displays chemical potentials of Ref. [5] converted to the present units.

λ	$\Delta\tau$	N_{iter}	E	μ	Virial	μ (Ref. [5])
1	0.05	394	1.031710720	1.048334727	0.000000000	
10	0.05	446	1.159916767	1.284404840	0.000000000	
50	0.05	432	1.522757628	1.876928940	0.000000003	1.8769285
500	0.05	348	3.053321507	4.131516887	0.000000004	4.1315165
1500	0.05	275	4.566073050	6.287095396	0.000000015	6.2870955
5000	0.02	533	7.251147655	10.07722612	−0.000000074	10.0772255
15000	0.01	890	11.16406435	15.57610963	−0.00000017	15.575140
25000	0.02	848	13.66678924	19.08763399	0.00000015	19.088632
100000	0.01	691	23.7247465	33.184802	0.000017	
	TF		23.6833	33.1567		

TABLE VI. Chemical potential μ and energy E with Hermite mesh (except at the last line) for the nonseparable external potential defined in Eq. (46).

V_0	λ	N	h	$\Delta\tau$	N_{iter}	E	μ	Virial
∞	1	20	0.8	0.05	287	1.530891280	1.560971500	0.000000020
	1000	30	0.8	0.05	176	6.308834870	8.670315391	0.000000049
100	1	20	0.8	0.05	275	1.525944363	1.555775730	0.000000019
	1000	30	0.8	0.05	161	6.214757020	8.506122662	0.000000137
10	1	20	0.8	0.05	303	1.480952622	1.508530825	0.000000095
	1000	40	1.0	0.05	316	5.345812523	6.979115000	0.000000024
1	1	30	2.1	0.05	5000	0.96601	0.96944	−0.00009
1 (sinc)	1	30	0.8	0.05	5000	0.96600	0.96944	0.00008

[Eq. (9)] is well satisfied, we think that the results of Ref. [5] are less accurate.

E. Nonseparable external potential

The present technique with factorization b does not depend on the use of oscillator external potentials. To illustrate this fact, we now consider the external potential

$$V_{\text{ext}} = V_0\left\{1 - \exp\left[-\frac{1}{2V_0}(\omega_x^2 x^2 + \omega_y^2 y^2 + \omega_z^2 z^2)\right]\right\}, \quad (46)$$

with $\omega_x = \omega_y = \omega_z = 1$. A Taylor expansion shows that this potential resembles the harmonic-oscillator trap around its minimum. However it does not confine the particles since it has a threshold at V_0.

The results for various nonlinear parameters are presented in Table VI. The virial theorem is given by Eq. (8). The conditions of the calculation are roughly interpolated from Table I.

For $V_0 \to \infty$, one recovers the oscillator case from Table III. This case is shown in the first two lines of the table. Let us start with $V_0 = 100$ and the Hermite mesh. The external potential is still deep. The fact that it tends to a finite limit should not play a significant role. Indeed, the energy and chemical potential are close to the oscillator values. They are slightly below because the potential is broader. The difference is larger for $\lambda = 1000$ since there are more bosons. The accuracy is slightly less good under the same conditions.

For $V_0 = 10$, the effect of the absence of confinement becomes more significant. At $\lambda = 1000$, the number of points and the scale parameter must be increased to keep the same level of accuracy. The condensate starts to be sensitive to the region where the potential is flat. For $V_0 = 1$, the convergence becomes very slow at $\lambda = 1$ in spite of a significant adjustment of the conditions of the calculation indicating an expansion of the condensate. The calculation was stopped after 5000 iterations. Both E and μ are now smaller. Their values are confirmed by a calculation with the sinc mesh. We could not obtain a significant result for $\lambda = 1000$. The trap is not deep enough to contain the increased number of bosons.

IV. CONCLUSION

The combination of the imaginary-time and Lagrange-mesh methods provides a simple, fast, and accurate way of solving the three-dimensional Gross-Pitaevskii equation. This is realized here with a fourth-order factorization of the exponential operator appearing in the imaginary-time method. The algorithm is not restricted to harmonic-oscillator trapping potentials. The virial theorem offers an efficient way of choosing the conditions of calculations adapted to the required accuracy. In general, it also provides an evaluation of the accuracy reached on the chemical potential. This accuracy is less good than the accuracy on the energy per boson which arises from a variational principle.

Calculations have been performed for λ ranging from 1 to 10^7. The calculation time increases with λ but remains quite short up to the highest values. The accuracy becomes less good at high λ values where the Thomas-Fermi approximation becomes accurate.

It will be interesting to extend the present approach to the time evolution of a condensate. The same ingredients should allow to accurately treat a number of such applications.

ACKNOWLEDGMENTS

This text presents research results of the Belgian program P6/23 on interuniversity attraction poles initiated by the Belgian-state Federal Services for Scientific, Technical and Cultural Affairs (FSTC).

APPENDIX

The calculation of $\nabla\psi$ is needed in the fourth-order algorithm. To this end, one calculates values of the first derivative of the Lagrange functions at the mesh points,

$$\lambda_j^{1/2} f_i'(u_j) = (-1)^{i-j}\frac{1}{u_j - u_i},$$

$$\lambda_i^{1/2} f_i'(u_i) = 0. \quad (A1)$$

Notice that these expressions are common for the Hermite and sinc meshes (but the zeros u_j are different). After parity projection they read

$$\lambda_j^{1/2} f_i^{p'}(u_j) = (-1)^{i-j}\left(\frac{1}{u_j - u_i} - \frac{p}{u_j + u_i}\right),$$

$$\lambda_i^{1/2} f_i^{p'}(u_i) = -\frac{p}{2u_i}. \tag{A2}$$

Hence the components of the gradient are approximated by

$$\frac{\partial \psi}{\partial x}(h_x u_i, h_y v_j, h_z w_k) = h_x^{-1} \sum_{i'=1/2}^{1/2(N_x-1)} c_{i'jk} \lambda_i^{1/2} f_{i'}^{p'_x}(u_i),$$

$$\frac{\partial \psi}{\partial y}(h_x u_i, h_y v_j, h_z w_k) = h_y^{-1} \sum_{j'=1/2}^{1/2(N_y-1)} c_{ij'k} \mu_j^{1/2} g_{j'}^{p'_y}(v_j),$$

$$\frac{\partial \psi}{\partial z}(h_x u_i, h_y v_j, h_z w_k) = h_z^{-1} \sum_{k'=1/2}^{1/2(N_z-1)} c_{ijk'} \nu_k^{1/2} h_{k'}^{p'_z}(w_k). \tag{A3}$$

[1] F. Dalfovo, S. Giorgini, L. P. Pitaevskii, and S. Stringari, Rev. Mod. Phys. **71**, 463 (1999).
[2] B. I. Schneider and D. L. Feder, Phys. Rev. A **59**, 2232 (1999).
[3] M. L. Chiofalo, S. Succi, and M. P. Tosi, Phys. Rev. E **62**, 7438 (2000).
[4] C. M. Dion and E. Cancès, Phys. Rev. E **67**, 046706 (2003).
[5] Y.-S. Choi, J. Javanainen, I. Koltracht, M. Kostrun, P. J. McKenna, and N. Savytska, J. Comput. Phys. **190**, 1 (2003).
[6] W. Bao, D. Jaksch, and P. A. Markowich, J. Comput. Phys. **187**, 318 (2003).
[7] D. McPeake and J. F. McCann, Comput. Phys. Commun. **161**, 119 (2004).
[8] S. A. Chin and E. Krotscheck, Phys. Rev. E **72**, 036705 (2005).
[9] C. M. Dion and E. Cancès, Comput. Phys. Commun. **177**, 787 (2007).
[10] S.-L. Chang, C.-S. Chien, and Z.-C. Li, Comput. Phys. Commun. **179**, 208 (2008).
[11] D. Baye and P. H. Heenen, J. Phys. A **19**, 2041 (1986).
[12] D. Baye, M. Hesse, and M. Vincke, Phys. Rev. E **65**, 026701 (2002).
[13] D. Baye, Phys. Status Solidi B **243**, 1095 (2006).
[14] M. Suzuki, Phys. Lett. A **146**, 319 (1990).
[15] M. Suzuki, J. Math. Phys. **32**, 400 (1991).
[16] S. Chin and C. Chen, J. Chem. Phys. **117**, 1409 (2002).
[17] I. P. Omelyan, I. M. Mryglod, and R. Folk, Phys. Rev. E **66**, 026701 (2002).
[18] D. Baye, G. Goldstein, and P. Capel, Phys. Lett. A **317**, 337 (2003).
[19] G. Goldstein and D. Baye, Phys. Rev. E **70**, 056703 (2004).
[20] M. Hesse and D. Baye, J. Phys. B **32**, 5605 (1999).
[21] M. Hesse and D. Baye, J. Phys. B **34**, 1425 (2001).
[22] M. Hesse and D. Baye, J. Phys. B **36**, 139 (2003).
[23] M. Vincke and D. Baye, J. Phys. B **39**, 2605 (2006).
[24] D. Baye, M. Vincke, and M. Hesse, J. Phys. B **41**, 055005 (2008).
[25] D. Baye and M. Vincke, Phys. Rev. E **59**, 7195 (1999).
[26] M. Abramowitz and I. A. Stegun, *Handbook of Mathematical Functions* (Dover, New York, 1965).
[27] P. A. Ruprecht, M. J. Holland, K. Burnett, and M. Edwards, Phys. Rev. A **51**, 4704 (1995).